

Detailed chemical abundance analysis of the thick disk star cluster Gaia 1 [★]

Andreas Koch^{1,2}, Terese T. Hansen³, and Andrea Kunder^{4,5}

¹ Department of Physics, Lancaster University, LA1 4YB, Lancaster, UK

² Zentrum für Astronomie der Universität Heidelberg, Astronomisches Recheninstitut, Mönchhofstr. 12, 69120 Heidelberg, Germany

³ Carnegie Observatories, 813 Santa Barbara St., Pasadena, CA 91101, USA

⁴ Leibniz-Institut für Astrophysik Potsdam, An der Sternwarte 16, 14482 Potsdam, Germany

⁵ Saint Martin's University, Old Main, 5000 Abbey Way SE, Lacey, WA 98503, USA

Received: 26 June 2017 / Accepted: 11 September 2017

ABSTRACT

Star clusters, particularly those objects in the disk-bulge-halo interface are as of yet poorly charted, albeit carrying important information about the formation and the structure of the Milky Way. Here, we present a detailed chemical abundance study of the recently discovered object Gaia 1. Photometry has previously suggested it as an intermediate-age, moderately metal-rich system, although the exact values for its age and metallicity remained ambiguous in the literature. We measured detailed chemical abundances of 14 elements in four red giant members, from high-resolution ($R=25000$) spectra that firmly establish Gaia 1 as an object associated with the thick disk. The resulting mean Fe abundance is $-0.62 \pm 0.03(\text{stat.}) \pm 0.10(\text{sys.})$ dex, which is more metal-poor than indicated by previous spectroscopy from the literature, but it is fully in line with values from isochrone fitting. We find that Gaia 1 is moderately enhanced in the α -elements, which allowed us to consolidate its membership with the thick disk via chemical tagging. The cluster's Fe-peak and neutron-capture elements are similar to those found across the metal-rich disks, where the latter indicate some level of s -process activity. No significant spread in iron nor in other heavy elements was detected, whereas we find evidence of light-element variations in Na, Mg, and Al. Nonetheless, the traditional Na-O and Mg-Al (anti-)correlations, typically seen in old globular clusters, are not seen in our data. This confirms that Gaia 1 is rather a massive and luminous open cluster than a low-mass globular cluster. Finally, orbital computations of the target stars bolster our chemical findings of Gaia 1's present-day membership with the thick disk, even though it remains unclear, which mechanisms put it in that place.

Key words. Stars: abundances – Galaxy: abundances – Galaxy: structure – Galaxy: disk – globular clusters – open clusters and associations: individual: Gaia 1

1. Introduction

Star clusters in our Milky Way are excellent testbeds to study the formation, evolution, and structure of the underlying Galactic components. When turning to low Galactic latitudes, not only the, primarily old, globular clusters (GCs) are of interest, but young-to-intermediate-age open clusters (OCs) become the prime tracer of the Galactic disks. Hence, a distinction between low-mass GCs and massive and luminous OCs is imperative. Likewise, establishing an association with either component can help with better charting the disk-bulge-halo interfaces in addition to studying their stellar content (e.g., Ness et al. 2013; Recio-Blanco et al. 2014; Koch et al. 2016, 2017).

Gaia 1 is a star cluster that was recently discovered by Koposov et al. (2017) in the first Gaia data release (Prusti et al. 2016), alongside with another system of lower mass. Its observation and previous detections were seriously hampered by the nearby bright star Sirius, which emphasized the impressive discovery power of the *Gaia* mission. This object was first characterized as an intermediate-age (6.3 Gyr) and moderately metal-rich (-0.7 dex) system, based on isochrone fits to a comprehensive combination of *Gaia*, 2MASS (Cutri et al. 2003), WISE

(Wright et al. 2010), and Pan-STARRS1 (Chambers et al. 2016) photometry. Thence, this object was characterized by Koposov et al. (2017) as a star cluster, most likely of the globular confession. Further investigation of Gaia 1 found a metallicity higher by more than 0.5 dex, which challenged the previous age measurement and rather characterized it as a young (3 Gyr), metal-rich (-0.1 dex) object, possibly of extragalactic origin given its orbit that leads it up to ~ 1.7 kpc above the disk (Simpson et al. 2017). Subsequently, Mucciarelli et al. (2017) measured chemical abundances of six stars in Gaia 1, suggesting an equally high metallicity, but based on their abundance study, the suggestion of an extragalactic origin was revoked. While a more metal-rich nature found by the latter authors conformed with the results by Simpson et al. (2017), the evolutionary diagrams of both studies are very dissimilar and could not be explained by one simple isochrone fit. In particular, it was noted that “the Simpson et al. (2017) stars do not define a red giant branch in the theoretical plane, suggesting that their parameters are not correct” (Fig. 1 of Mucciarelli et al. 2017). Such an inconsistency clearly emphasizes that a clear-cut chemical abundance scale is inevitable for fully characterising Gaia 1, and to further allow for tailored age determinations, even more so in the light of the seemingly well-determined orbital characteristics. Thus, this work focuses on a detailed chemical abundance analysis of four red giant members of Gaia 1, based on high-resolution spectroscopy, which we complement by an investigation of the orbital properties of

Send offprint requests to: A. Koch; e-mail: a.koch1@lancaster.ac.uk

[★] This paper includes data gathered with the 2.5 meter du Pont Telescope located at Las Campanas Observatory, Chile.

this transition object. Combined with the red clump sample of Mucciarelli et al. (2017) and reaching down to the subgiant level (Simpson et al. 2017), stars in different evolutionary states in Gaia 1 are progressively being sampled.

This paper is organized as follows: In Sect. 2 we present our data acquisition and reduction, followed by a description of the ensuing chemical abundance analysis in Sect. 3. The results thereof are presented in Sect. 4. In Sect. 5, we introduce our orbital computations for Gaia 1 before concluding on our results in Sect. 6.

2. Observations

Targets for our spectroscopy were selected from the Two Micron All Sky Survey (2MASS) catalog (Cutri et al. 2003) within an identical, fiducial spatial selection region as in Koposov et al. (2017, see Fig. 1). None of our targets overlap with the recent intermediate-resolution sample of Simpson et al. (2017)¹.

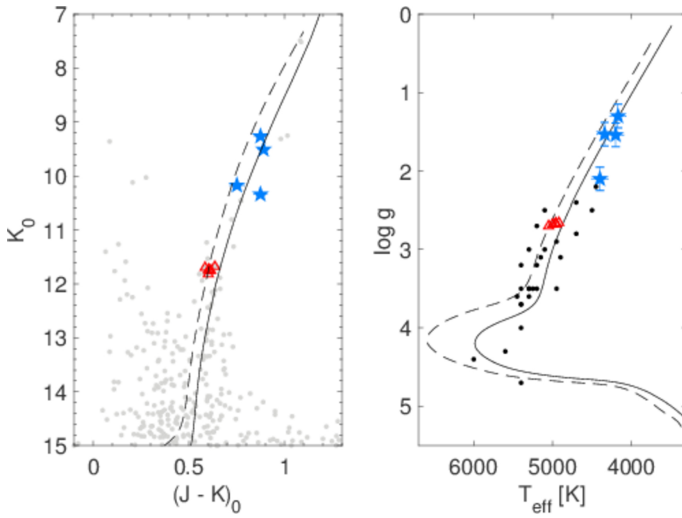


Fig. 1. Left panel: Colour magnitude diagram from 2MASS of stars within ~ 2 half-light radii of Gaia 1 (gray points). Right panel: Hertzsprung-Russell diagram, constructed from our best spectroscopic stellar parameters. Our targets are highlighted in blue, red triangles are the He-clump targets of Mucciarelli et al. (2017), and the sample of Simpson et al. (2017) is shown in black. Either panel also displays Dartmouth isochrones (Dotter et al. 2008) using an age (6.3 Gyr) and metallicity (-0.7 dex), as suggested by Koposov et al. (2017, dashed line), and one with 12 Gyr and -0.65 dex (solid line).

Observations of four candidate members were taken during four nights in March 2017 using the Echelle spectrograph at the 2.5-m du Pont telescope at the Las Campanas Observatory, Chile, with a seeing of $0.7''$ – $1.0''$ throughout the nights. Our spectroscopic set-up included a $1.0''$ slit with 2×1 binning in spectral and spatial dimensions, resulting in a resolving power of $R \sim 25000$. An observing log is given in Table 1. Despite the proximity to the nearby star Sirius, the location of our targets at $10'$ – $12'$ from this bright ($V = -1.5$ mag) object ensured that no

stray light contaminated our spectra. In fact, no evidence for any flux from Sirius is seen in our data, which would show up, e.g., in the form of blue-shifted Balmer lines ($v_{\text{Sir}} = -5 \text{ km s}^{-1}$ vs. $\sim 57 \text{ km s}^{-1}$ for the GC stars) and/or an excess flux in the blue range, as Sirius' spectral type is A1V.

The data were reduced using the Carnegie Python Distribution² (Kelson 1998, 2003; Kelson et al. 2000). Subtraction of sky and scattered background light was carefully treated by the software and aided by our use of a slit length of $4''$ and no binning in spatial direction (see also Sect. 4.1.2). The final spectra cover a full spectral range of 3340 – 8850 \AA . Typical signal-to-noise (S/N) ratios reach 70 px^{-1} in the peak of the order containing $H\alpha$ and decline towards 25 px^{-1} in the bluer orders around 4500 \AA (Table 1). All four stars are radial velocity members of Gaia 1, and we will further discuss its kinematic properties in Sect. 5.1.

3. Abundance analysis

Throughout the analysis we employed standard techniques as in our previous works (e.g., Koch & McWilliam 2014). In brief, equivalent widths (EWs) were measured by fitting Gaussian line profiles within IRAF's *splot* environment. To this end, we used the line list from Ruchti et al. (2016) with updated $\log g f$ values for Mg from Pehlivan Rhodin et al. (2017) and accounting for hyperfine splitting for odd-Z elements. Due to the blending of features at the higher metallicity of the stars, we employed spectral synthesis for C, Ba, and Eu. The measurements of individual lines are summarized in Table 2.

All further analyses employed the 2014 version of the stellar abundance code MOOG (Snedden 1973). As for the model atmospheres, we interpolated Kurucz's grid³ of one-dimensional 72-layer, plane-parallel, line-blanketed models without convective overshoot, and assuming that local thermodynamic equilibrium (LTE) holds for all species. This model grid further incorporated the α -enhanced opacity distributions, AODFNEW (Castelli & Kurucz 2004). Finally, all abundances were placed on the solar, photospheric scale of Asplund et al. (2009).

3.1. Stellar parameters

For an initial estimate of the stellar temperature, we employed the calibrations for giants of Alonso et al. (1999) using JHK 2MASS photometry, which, in turn, was converted to the TCS system needed for these calibrations. The reddening maps of Schlafly & Finkbeiner (2011) indicate an $E(B-V) = 0.49$ mag with negligible variation amongst the four targets. Finally, for the metallicity to enter the colour- T_{eff} relations we estimated the value from the isochrone fits of Koposov et al. (2017), namely $[\text{Fe}/\text{H}] = -0.7$ dex. As a result, the temperatures from the $(J-K)$ and $(J-H)$ colour-indices agree to within 55 K , with the same order of 1σ scatter. This compares to a typical error on the colour-temperatures of 70 – 140 K . Our photometric temperatures are listed in Table 3, alongside all other stellar parameters of our sample.

Next, T_{eff} was further refined by requiring excitation equilibrium of neutral iron lines, where we culled too strong and the weakest lines from consideration by requiring $-5.5 \leq \log \text{EW}/\lambda \leq -4.5$. Furthermore, we restricted this part of the analysis to wavelengths redder than 5200 \AA owing to the

¹ We note that the target source identification of the stars in the Tables B.1 and B.2 of Simpson et al. (2017) is wrong in that there are no have cross-matches in the *Gaia* archive. The correct identifiers can be found in the csv tables provided by the authors in the preprint version of their paper (<https://arxiv.org/e-print/1703.03823v1>).

² <http://code.obs.carnegiescience.edu/>

³ <http://kurucz.harvard.edu/grids.html>

Table 1. Observing log and target properties

Star	α (J2000.0)	δ (J2000.0)	J [mag]	H [mag]	K [mag]	Date of observation	t_{exp} [s]	SN^a [px $^{-1}$]	v_{HC} [km s $^{-1}$]
1	06:45:49.77	−16:44:46.47	10.550	9.700	9.440	06 Mar 2017	3×1500	70/44/14	56.3±0.3
2	06:45:57.64	−16:40:11.00	10.816	9.965	9.687	07 Mar 2017	3×1500	70/44/14	56.9±0.3
3	06:45:53.81	−16:45:32.21	11.337	10.564	10.350	08 Mar 2017	3×1500	50/30/9	62.0±0.3
4	06:45:55.93	−16:43:46.98	11.628	10.753	10.518	09 Mar 2017	3×1500	40/25/6	53.5±0.3

Notes. ^(a) Measured at 6550/5500/4500 Å.

Table 2. Line list

Element	λ [Å]	E.P. [eV]	$\log g f$	EW [m Å]			
				1	2	3	4
O I	6300.30	0.000	−9.715	67	67	59	48
O I	6363.78	0.020	−10.190	27	16	32	...
Na I	5682.63	2.102	−0.706	171	170	171	146
Na I	5688.21	2.104	−0.404	192	178	174	164
Na I	6154.23	2.102	−1.547	115	116	113	68
Na I	6160.75	2.104	−1.246	125	121	135	100

Notes. Table 2 is available in its entirety in electronic form via the CDS.

Table 3. Stellar parameters

Star	T_{eff} [K]			$\log g$ [dex]	ξ [km s $^{-1}$]
	(J–H)	(J–K)	(spec.)		
1	4160	4081	4170	1.30	2.0
2	4169	4047	4200	1.54	2.0
3	4383	4368	4340	1.53	2.0
4	4086	4083	4400	2.07	2.0

increasing noise at the bluer end. The resulting spectroscopic temperatures could be typically determined to within 100 K (based on the line-to-line scatter in comparison with the change of slopes) and are in excellent agreement with the photometric ones, with the exception of star #4, which shows a colder photometric colour. For the remainder of the analysis we used the spectroscopic values as the final T_{eff} in the atmospheres.

In the next step, photometric gravities were determined by adopting the above temperatures, a distance to Gaia 1 of 4.6 kpc (Koposov et al. 2017) and assuming a typical mass of the stars on the RGB of 1.0 M_{\odot} , as indicated by an intermediate-age, metal-rich Dartmouth isochrone (Dotter et al. 2008) based on the stellar population identified by Koposov et al. (2017). By enforcing ionization equilibrium between neutral and ionized iron lines, we were also able to estimate spectroscopic surface gravities, which are in good agreement with the photometric ones. The implications of our refined $\log g$ will be discussed further in Sect. 5.

Finally, the microturbulence was fixed by removing the trend of the abundance from neutral iron lines with reduced width, $\log \text{EW}/\lambda$. As before, weak lines were removed from this exercise using the same cuts as mentioned above, since they are increasingly prone to noise. Likewise, strong lines were deemed unsuitable due to their saturation on the flat part of the curve of growth (Magain 1984; Hanke et al. 2017). Overall, the resulting abundance trend was not very sensitive to the choice of microturbulence, placing all our stars around values of 2.0 ± 0.2 km s $^{-1}$.

3.2. Abundance errors

Also for the abundance errors we followed a standard approach. To this end, statistical errors were adopted via the line-to-line scatter from multiple line measurements, which we list as σ in Table 4, together with the number of lines, N , that were measured. The systematic errors, in turn, were quantified via variations of the stellar atmosphere parameters. Thus we computed new abundances after varying each parameter independently about their uncertainty, i.e., $T_{\text{eff}} \pm 100$ K; $\log g \pm 0.15$ dex; $\xi \pm 0.2$ km s $^{-1}$; $[\text{M}/\text{H}] \pm 0.1$ dex, and switching from the α -enhanced opacity distributions to the Solar-scaled values. For the latter we adapted half the abundance change as the implied error, mimicking an uncertainty in the atmospheres' $[\alpha/\text{Fe}]$ ratio of ± 0.2 dex. All respective changes and the overall result, obtained by adding the contributions in quadrature, are summarized in Table 5, exemplary for star #1.

4. Abundance results

All abundance ratios are summarized in Table 4.

4.1. Iron

From our abundance analysis of the four Gaia 1 stars we found a mean iron abundance of -0.62 ± 0.03 (stat.) ± 0.10 (sys.) dex. Here, ionization equilibrium has been achieved per construction in that we forced the Fe I and Fe II abundances to agree in order to determine spectroscopic gravities. The 1σ dispersion of our $[\text{Fe}/\text{H}]$ is 0.05 ± 0.02 dex, a low value fully in line with other stellar systems of similarly low mass ($2.2 \times 10^4 M_{\odot}$; $M_V \sim -5$ mag; Carretta et al. 2009a; Pancino et al. 2010; Koch et al. 2012). The moderately metal-rich value we found is in excellent agreement with the isochrone fitting of Koposov et al. (2017), who adopted an intermediate age of the GC of 6.3 Gyr. However, the latter should be taken with caution, given the uncertain reddening of the cluster (Mucciarelli et al. 2017) and the fact that the metallicity sensitivity of the RGB relies entirely on its colour. In addition, the available ground-based photometry does not reach below the metallicity- and age-sensitive turn-off, which would allow for an understanding of its CMD morphology, and it is affected badly by the presence of Sirius. Future *Gaia* releases will provide a better grip on the CMD of this cluster.

4.1.1. Comparison with medium-resolution literature results

In stark contrast, Simpson et al. (2017) found a much more metal-rich value of -0.13 ± 0.13 dex using two approaches on 27 red clump member candidates. These comprised an analysis at similar spectral resolution to the present work, but employing a smaller wavelength range, complemented by calcium triplet (CaT) spectroscopy at low resolution ($R \sim 10000$). The cause for

Table 4. Abundance results

Element ^a	1			2			3			4			Gaia 1	
	[X/Fe]	σ	N	[X/Fe]	σ	N	[X/Fe]	σ	N	[X/Fe]	σ	N	[X/Fe] ^c	σ^c
Fe I	-0.67	0.21	97	-0.55	0.22	89	-0.67	0.24	94	-0.60	0.28	88	-0.62±0.03	0.05±0.02
Fe II	-0.66	0.33	9	-0.54	0.27	9	-0.66	0.22	9	-0.61	0.22	7	-0.61±0.08	0.00±0.08
C I ^b	-0.21	0.40	...	-0.53	0.40	...	-0.38	0.40	...	-0.85	0.40	...	-0.49±0.20	0.00±0.25
O I	0.36	0.03	2	0.25	0.15	2	0.49	0.10	2	0.50	...	1	0.41±0.04	0.06±0.04
Na I ^{LTE}	0.53	0.07	4	0.36	0.14	4	0.64	0.18	4	0.24	0.06	4	0.43±0.08	0.14±0.06
Na I ^{NLTE}	0.38	0.08	4	0.21	0.16	4	0.48	0.16	4	0.10	0.06	4	0.29±0.07	0.14±0.06
Mg I	0.41	0.20	8	0.15	0.17	7	0.29	0.23	7	0.14	0.19	7	0.24±0.06	0.09±0.05
Al I	0.64	...	1	0.46	...	1	0.31	...	1	0.46	...	1	0.47±0.06	0.11±0.05
Si I	0.36	0.27	17	0.31	0.36	17	0.35	0.30	15	0.26	0.27	16	0.32±0.04	0.00±0.05
Ca I	0.22	0.29	14	0.04	0.29	13	0.25	0.35	13	0.19	0.34	14	0.17±0.04	0.00±0.09
Sc II	0.05	0.23	4	0.17	0.13	4	0.13	0.29	3	0.01	0.07	3	0.07±0.05	0.05±0.05
Ti I	0.35	0.36	28	0.17	0.20	21	0.11	0.14	23	0.22	0.24	20	0.20±0.04	0.07±0.04
Ti II	0.14	0.23	5	-0.07	0.18	4	-0.09	0.09	4	-0.16	0.06	3	-0.09±0.05	0.05±0.06
Cr I	0.16	0.26	10	-0.14	0.27	10	-0.08	0.19	9	0.04	0.29	10	-0.01±0.06	0.08±0.06
Co I	0.25	0.29	7	0.04	0.21	7	0.13	0.35	6	0.30	0.27	4	0.15±0.06	0.04±0.10
Ni I	0.08	0.35	36	-0.02	0.35	37	0.02	0.31	36	-0.01	0.30	32	0.02±0.05	0.00±0.05
Ba II	-0.18	0.07	3	-0.14	0.08	3	-0.22	0.07	3	-0.04	0.10	3	-0.18±0.07	0.00±0.07
Eu II	0.11	0.05	1	0.05	0.05	1	0.12	0.10	0	0.28	0.15	1	0.11±0.05	0.00±0.05

Notes. ^(a) Ionised species are given relative to Fe II. Abundance ratios are listed relative to iron, except for Fe I and Fe II (relative to H). ^(b) From the CH G-band. ^(c) Mean and 1 σ -dispersion of the entire cluster based on an error-weighted maximum likelihood approach.**Table 5.** Systematic errors for Star 1

Element	T _{eff} ±100 K	log g ±0.15 dex	ξ ±0.2 km s ⁻¹	[M/H] ±0.1 dex	ODF	$\sigma_{\text{sys,tot}}$
Fe I	<0.01	±0.03	±0.09	±0.02	-0.07	0.10
Fe II	±0.16	±0.07	±0.04	±0.03	-0.16	0.20
C I	±0.19	±0.08	±0.14	<0.01	-0.08	0.26
O I	±0.02	±0.06	<0.01	±0.04	-0.12	0.10
Na I	±0.09	±0.01	±0.10	<0.01	-0.03	0.13
Mg I	±0.03	<0.01	±0.05	±0.02	-0.06	0.07
Al I	±0.05	<0.01	±0.03	<0.01	-0.02	0.06
Si I	±0.09	±0.03	±0.03	±0.02	-0.09	0.11
Ca I	±0.11	±0.01	±0.14	<0.01	-0.05	0.18
Sc II	±0.03	±0.06	±0.06	±0.03	-0.13	0.11
Ti I	±0.16	<0.01	±0.14	<0.01	-0.06	0.22
Ti II	±0.03	±0.06	±0.13	±0.03	-0.13	0.16
Cr I	±0.13	<0.01	±0.09	<0.01	-0.05	0.16
Co I	±0.08	<0.01	±0.13	±0.02	-0.07	0.16
Ni I	<0.01	±0.04	±0.10	±0.02	-0.09	0.11
Ba II	±0.02	±0.04	±0.11	±0.04	-0.16	0.15
Eu II	±0.02	±0.06	±0.04	±0.03	-0.12	0.10

these very high metallicities from the high-resolution spectra lies beyond the scope of our analysis, but reasons could be related to S/N, which is listed down to negative values in Simpson et al. (2017, their Table B.1). We can furthermore conjecture on the employed CaT calibrations in that study (valid up to [Fe/H]=0.5, but dependent on stellar luminosity) or residual foreground contamination, for which the CaT calibrations cannot be applied. Furthermore, the majority of AAOMega targets in that study are stars on the lower RGB and subgiants, for which the CaT calibrations have only have limited applicability. Combined with the ambiguous target identification mentioned above (Sect. 2) and Mucciarelli et al. (2017)’s suggestion of wrong stellar parameters in that study, these results are difficult to reconcile with our measurements.

4.1.2. Comparison with high-resolution literature results

Recently, Mucciarelli et al. (2017) performed an abundance analysis of six He-clump stars in Gaia 1 at a data quality comparable to our study, albeit at higher resolution of 36000. Their main conclusion was that Gaia 1 is a disk object at Solar metallicity with Solar-scaled abundance ratios. While the metal-rich nature found by these authors conformed with the results by Simpson et al. (2017), the HRD of both studies are very dissimilar and could not be explained by a simple isochrone fit. In particular, it was noted that “the Simpson et al. (2017) stars do not define an RGB in the theoretical plane, suggesting that their parameters are not correct” (Fig. 1 of Mucciarelli et al. 2017, and Fig. 1 in our present work). Such an inconsistency clearly emphasizes that age and metallicity derivations are vital, and we suggest that a lower metallicity as found in our analysis would be able to resolve the discrepancy with the literature values.

Instrumental effects

In order to test, whether the discrepant metallicity scales are an instrumental artefact, we thoroughly checked the background subtraction performance of our data. The typical sky level is $\sim 12\text{--}14\%$ of the object flux in the center of the orders around 6000 \AA so that poor sky subtraction would have rendered our EWs lower by a factor of up to 0.85, leading to even lower measured metallicities. Conversely, we would need to increase our EWs by 44% to reach the Solar iron abundance measured by Mucciarelli et al. (2017), whereas both their and our studies reached a much higher accuracy. Due to our used slit length of $4''$ and no binning in the spatial direction, the subtraction of sky and scattered light (note, e.g., a possible contribution from a 79% moon at 36°) was fully removed by our reduction procedures (Kelson 1998, 2003; Kelson et al. 2000)⁴.

Mass loss

Asserting that the two abundance scales established by Mucciarelli et al. (2017) and ourselves are real, we need to consider the option that Gaia 1 hosts two stellar populations – one metal-rich (\sim Solar) and one metal-poor (~ -0.6 dex). Since Mucciarelli et al. (2017) focused on the He-burning red clump, which is, by definition, young and metal-rich, their study would have missed the presence of the metal-poor population that showed up in our RGB sample.

This scenario, however, is uncomfortable given the system's low mass. Multiple populations of such distinction are mainly found in massive systems (e.g., Lee et al. 2009; Johnson & Pilachowski 2010; Marino et al. 2015), also towards the Galactic plane (e.g., Mauro et al. 2012; Origlia et al. 2013), which, in light of Gaia 1's rather low mass would imply that it has lost a great deal of mass. This was deemed unrealistic by Mucciarelli et al. (2017) given the cluster's purported young age of 3–6 Gyr, while an older age cannot be ruled out by isochrones of a lower metallicity and higher age (Fig. 1). Moreover, the lack of a Na-O anti-correlation (Sect. 4.3) appears to argue against a more massive origin of Gaia 1.

4.2. Light elements: Li, C

While we were able to obtain upper limits for the lithium abundance from synthesis of the 6707 \AA resonance line, the low values of typically $A(\text{Li}) < -0.3$ reflect the expected depletion seen in evolved giants (Spite & Spite 1982; Lind et al. 2009). We do not consider this fragile element any further.

Carbon abundances were derived from synthesis of the CH band at 4300 \AA , using the line list from Masseron et al. (2014). We find carbon abundances that are much lower than typical Galactic stars from the literature (e.g., Nissen et al. 2014), but those samples are mostly based on dwarfs, while our evolved giants ($\log(L/L_\odot) \sim 2\text{--}2.6$) need to be corrected for evolutionary status (Placco et al. 2014). Such corrections for metal-poor stars with similar T_{eff} and $\log g$ are as large as 0.7 dex, which would place our stars with solar (or slightly enhanced) carbon abundances.

⁴ Since our observations were taken during the same nights as those of Mucciarelli et al. (2017), this would have affected both data sets in an identical manner.

4.3. Light element variations: O, Na, Mg, Al

For determining O-abundances, we made use of the, generally strong, [O I] 6300 and 6363 \AA lines. Na abundances were derived from four transitions, neglecting the strong NaD lines. Each measurement was corrected for NLTE effects using the calculations of Lind et al. (2011) in order to aid a fair comparison with the literature. Finally, our Al-abundance is based on the EW of the moderately strong ($50\text{--}80\text{ m\AA}$) 6698 \AA line.

Highlighted in Fig. 2 are the probability distributions for the mean value (here taken relative to the nominal sample mean, $\langle [X/\text{Fe}] \rangle$, to emphasize the actual abundance spreads) and the 1σ dispersion over our entire sample, in each measured element, accounting for the individual measurement errors. The mean and dispersions for the entire cluster are also listed in Table 4.

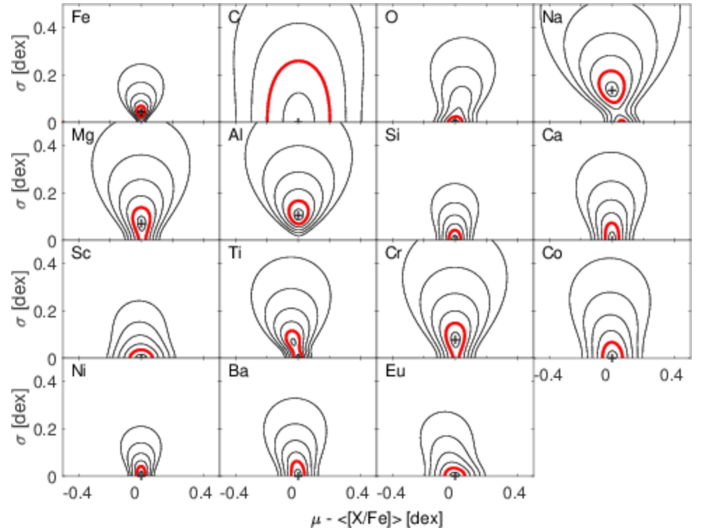


Fig. 2. Probability distributions of the mean values (μ) and dispersions (σ) in the abundance ratios. Here, the x-axis has been normalized to zero at the observed mean of each element's $[X/\text{Fe}]$ to emphasize the abundance spreads. Contours are placed at $0.5\text{--}3\sigma$ in steps of 0.5, where the red curve highlights the 1σ contour. Note the significant spreads in the light elements Na, Mg, and Al.

As expected for a chemically homogeneous system such as a star cluster, most elements have dispersions consistent with zero, i.e., any spread is driven by the measurement errors. The clear exceptions are those light elements that commonly partake in the proton-capture reactions in massive stars, i.e., Mg, Na, Al with a significant non-zero spread.

In Fig. 3 we further explore (anti-)correlations between these light elements that are found in the majority of Galactic GCs as a consequence of hot proton-burning reactions in a first generation of massive stars. These trends, however, are markedly lacking in Galactic field and OC stars, and in dwarf galaxies (Geisler et al. 2007). As Fig. 3 implies, there is no pronounced anti-correlation in Gaia 1, although both Na and O show a broad spread. Thus we see, chemically, no evidence for any multiple populations in our sample alone, while arguably this can also be driven by the low number of targets. Likewise, no significant Mg-Al correlation is seen in our data, although this trend is generally much weaker in the GCs than the more prominent Na-O relation, to the point, where it breaks down for the lowest-mass

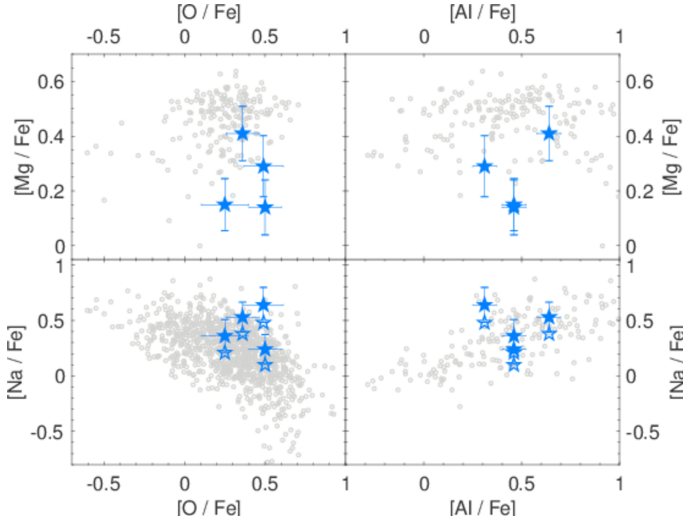


Fig. 3. Juxtaposition of various light element (anti-) correlations. GC stars from Carretta et al. (2009b) are indicated as gray circles, while our measurements are shown in blue. Here, open symbols are the NLTE-corrected values (Na) to aid a fair comparison with the literature. The correlations in Gaia 1 are weak, but a large spread in all elements is clearly visible.

systems and/or at the metal-rich tail of the GC population (e.g., Pancino et al. 2017).

At a present stellar mass of a few $10^4 M_{\odot}$, Gaia 1 lies at the boundary between a very low-mass GC and a very massive OC (e.g., Bragaglia et al. 2012), which corroborates previous findings of a threshold cluster mass, below which light element correlations are not detected (Carretta et al. 2010). In this context, Pancino et al. (2010) note that no evidence of light element variations in excess of $\lesssim 0.2$ dex is seen in their sample of OCs. Interestingly, the apparent lack of a Na-O anti-correlation, despite the presence of abundance spreads in Na and Al, in a sample of seven stars in the bulge GC NGC 6440 (Muñoz et al. 2017), closely resembles our finding in Gaia 1. Although, at $5.7 \times 10^5 M_{\odot}$, the former is more massive than Gaia 1 by a factor of several tens, this bolsters the suggestion of Muñoz et al. (2017) that some bulge clusters underwent a chemical evolution different from the rest of the Milky Way GC population. If Gaia 1 had developed from a once more massive system, which is feasible given the potential bimodal metallicity distribution, its progenitor could have resembled the massive NGC 6440 with its lack of a Na-O relation.

4.4. α -elements: Mg, Si, Ca, Ti

In Figs. 4–8 we overplot our measurements on literature data for various Galactic components. Specifically, these contain disk stars from Koch & Edvardsson (2002); Reddy et al. (2003, 2006); Bensby et al. (2014); Battistini & Bensby (2016), and bulge samples from Johnson et al. (2012); Bensby et al. (2013); Johnson et al. (2014); Van der Swaelmen et al. (2016).

Gaia 1 is moderately α -enhanced to 0.2–0.3 dex, depending on the exact element considered, thereby reflecting the different contributing nucleosynthetic channels. Its location in abundance space is shown in Fig. 4 in comparison with the Galactic disks and bulge. The [Ca/Fe] abundance ratios are systematically lower than the remaining elements, where the largest values of ~ 0.3 dex are reached for Si. The elevated $[\alpha/\text{Fe}]$ ratios are broadly consistent with a significant contribution from SNe II.

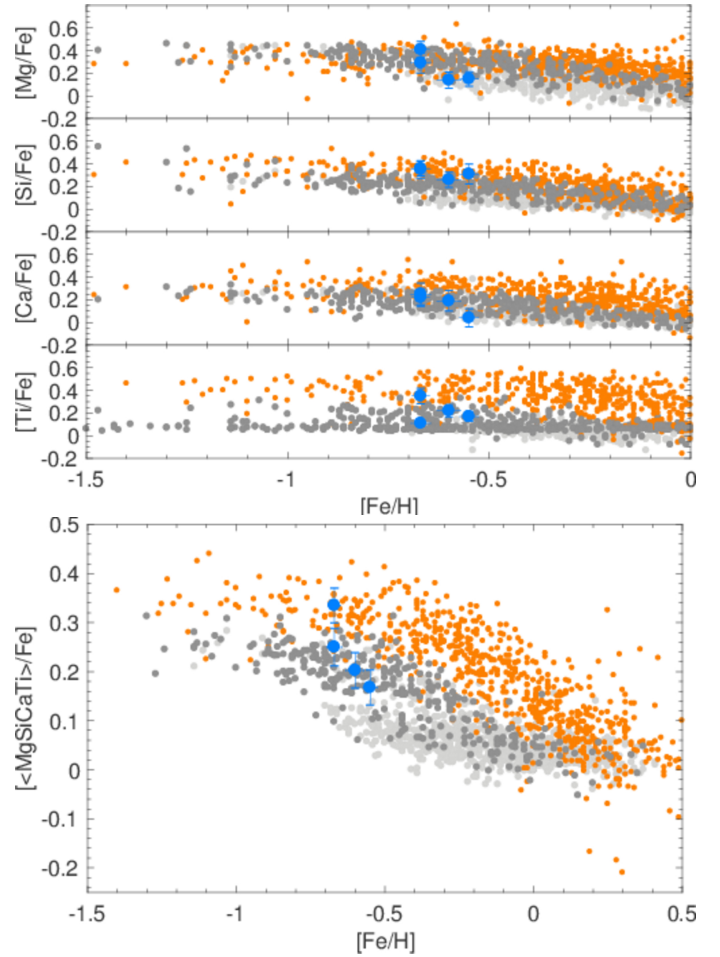


Fig. 4. Abundance ratios of the α -elements. Our stars are shown as blue symbols. Orange dots denote bulge stars from Gonzalez et al. (2011); Bensby et al. (2013); Johnson et al. (2014), while disk stars are depicted as gray points (Reddy et al. 2003, 2006; Bensby et al. 2014). Here, we specifically distinguish between thin (light gray) and thick disk stars (dark gray). The bottom panel shows the straight average of the Mg, Si, Ca, and Ti abundances as a proxy for α -enhancement. In all panels, the axis have been truncated to highlight the abundance region of our targets.

If we simplistically average over all four elements (bottom panel of Fig. 4), disregarding the difference in their hydrostatic vs. explosive nature (cf. Koch & McWilliam 2008; McWilliam 2016), we find a mean α -enhancement of $[<\text{Mg, Si, Ca, Ti}>/\text{Fe}] = 0.24 \pm 0.03$ dex with a 1σ spread of 0.05 ± 0.03 dex. Considering that the latter is predominantly driven by a significant spread in Mg as a consequence of the proton-capture reactions within the Mg-Al cycle, this provides no evidence of any spread in the majority of α -elements.

Fig. 4 (bottom) shows a clear separation of the Galactic components. Here, the literature values of Reddy et al. (2006) and Bensby et al. (2014) allowed for a unique separation into the thin and thick disks purely based on stellar kinematics (see also Rojas-Arriagada et al. 2017; Feltzing & Chiba 2013, and references therein). This comparison leaves little doubt about Gaia 1 being associated with the thick disk in terms of its moderate enhancement between the values in bulge stars (near the halo plateau of ~ 0.4 dex) and the thin disk abundances, only slightly in excess of Solar values. Here we note that this kind of comparison does not account for spatial variations in the literature

samples, ignoring the effects of any possible metallicity gradients (e.g., Janes 1979; Chen et al. 2003; Magrini et al. 2009; Cunha et al. 2016; Reddy et al. 2016).

Likewise, we do not detect any significant spreads in Si or Ca, as has been suggested for some bulge and (metal-poor) halo GCs as a consequence of leakage of protons from the Mg-Al chain in massive stars (Carretta et al. 2009b; Hanke et al. 2017; Muñoz et al. 2017).

4.5. Fe-peak elements: Sc, V, Cr, Co, Ni, Zn

Fig. 5 shows our measurements for the Fe-peak elements Sc, Cr, Co, and Ni along with the literature data for the bulge and thin and thick disk. None of these has been corrected for effects of NLTE, as none of the reference sets has been. Corrections for Cr are expected to be negligible in our stars (Bergemann & Cescutti 2010), while Co-abundances have NLTE corrections as high as 0.3 dex in thick disk stars, albeit at higher T_{eff} (~ 6000 K) than in our sample, or even up to 0.6 dex for cool, metal-poor halo stars (Bergemann et al. 2010).

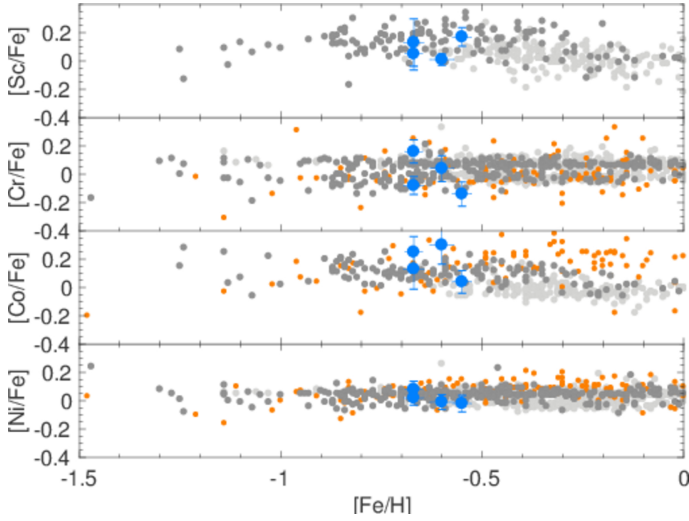


Fig. 5. Same as Fig. 4, but for the Fe-peak elements.

The majority of Fe-peak elements are coproduced in SNe Ia explosions alongside iron and their abundances should reflect this trend, irrespective of their environment. As seen in Fig. 5, this is indeed the fact in our Gaia 1 stars, although no sharp division is seen with respect to the Galactic components for the case of Ni and Cr. While Fig. 5 seems to imply the presence of a significant spread in the Cr-abundances, there is no obvious physical cause for such a dispersion, also in comparison with elements that undergo similar nucleosynthetic formation mechanisms; this rather hints that we underestimated the measurement errors for Cr or small, residual NLTE corrections that differ amongst our stars.

Nissen et al. (2000) ascertained that Sc behaves like an α -element in Galactic disk and halo stars, following a decreasing trend towards higher metallicities in the disks and showing a dichotomy in the halo, as also seen in terms of the dual high- and low- α components of the Milky Way (Nissen & Schuster 2010). This general trend is corroborated by our data and an overlap of Gaia 1 with the disk samples is clearly visible, although no clear cut between the various subcomponents beyond the measurement uncertainties can be established.

Overall, we are left with the conclusion that the material that Gaia 1 formed from was salted by SNe I ejecta to the same amount as typical of its environment, irrespective of its position in the Galaxy, or its age.

4.6. Neutron-capture elements: Ba, Eu

In order to derive abundances of the heavy elements Ba and Eu we resorted to spectral synthesis. For Ba, we adopted the error-weighted mean of the three strong, yet unsaturated, lines at 5853, 6164, and 6496 Å as the final [Ba/Fe] ratio, while the value for Eu was obtained from the overall weaker feature at 6645 Å. The results are presented in Fig. 6.

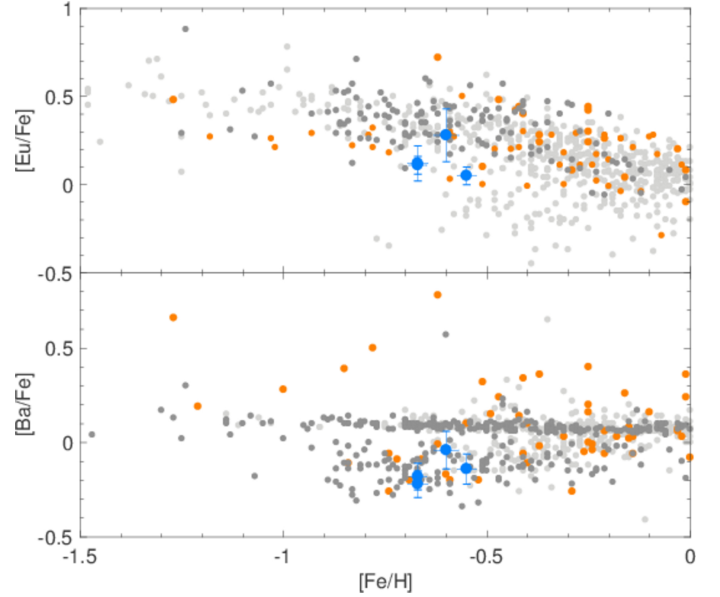


Fig. 6. Same as Fig. 4 but for the n -capture elements Ba and Eu.

As an r -process element, Eu is primarily produced in type II supernovae (SNe II) or via neutron star mergers (Woosley & Weaver 1995; Freiburghaus et al. 1999). Given the different timescales involved with those events compared to the slow evolution of SNe Ia that are responsible for the bulk of Fe-production, also the [Eu/Fe] ratio sees a decline from elevated values at the metal-poor end to (sub-)solar ratios for the more metal-rich components. Gaia 1 has Eu-abundances that follow this trend, albeit skimming the lower edge of the distribution.

Compared to the α -elements the respective Galactic chemical evolution of neutron capture elements is more complex, leading to a larger scatter in the heavy element abundances at a given metallicity (e.g., Sneden et al. 2008; Hansen et al. 2014). Nonetheless, combining the two chemical tracers into a simplistic $[(\alpha+Eu)/Fe]$ ratio has been shown to have a large discriminatory power between the kinematically selected thin and thick disks (Navarro et al. 2011). This is indicated in Fig. 7, where we overplot our measurements of Gaia 1 on the literature samples as before. With the possible exception of star #2, our targets in the Gaia 1 cluster are highly indicative of a thick disk association, as already evidenced by the other chemical tracers discussed above.

Barium is produced in the r -process at low metallicities, with ever-growing contributions from the s -process with increasing metallicities above $[Fe/H] \gtrsim -2.4$ (Busso et al. 1999; Simmerer et al. 2004; Karakas & Lattanzio 2014). As with Eu above, the

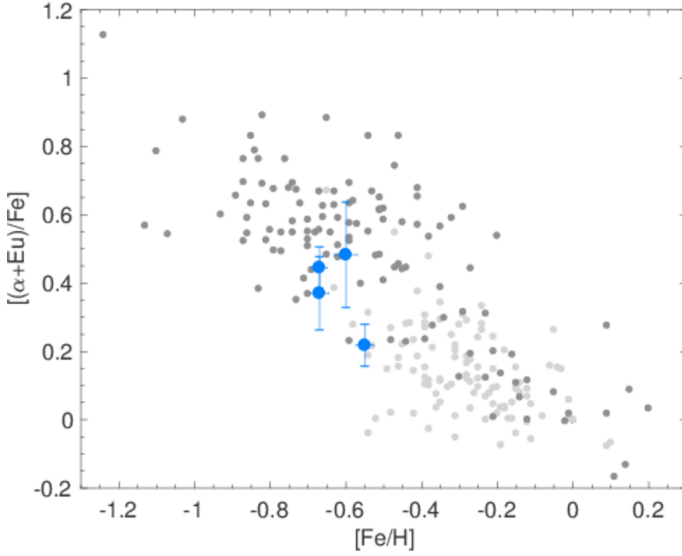


Fig. 7. Combination of the averaged α -element abundances with the r -process element Eu, following Navarro et al. (2011), for the thick and thin disk samples of Reddy et al. (2003, 2006).

Gaia 1 stars populate the lower branch seen in the $[\text{Ba}/\text{Fe}]$ abundance distribution (lower panel of Fig. 6).

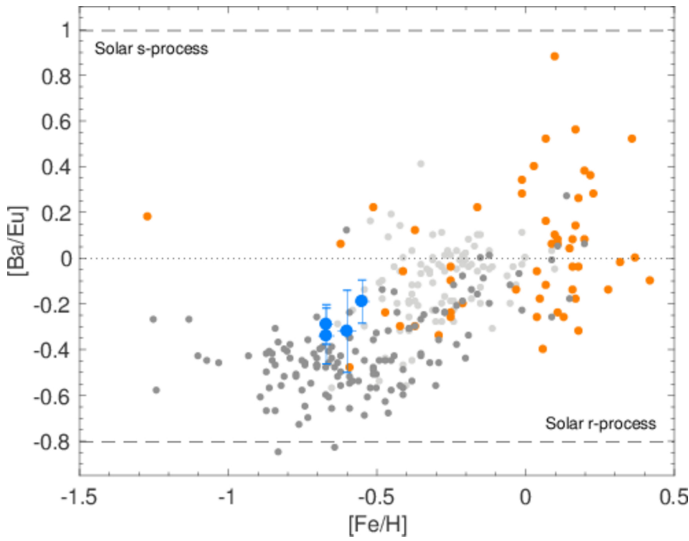


Fig. 8. The s -to- r -ratio $[\text{Ba}/\text{Eu}]$ for the same Galactic samples as shown in the previous figures. The Solar values are from Simmerer et al. (2004).

As is typical for moderately metal-poor disk stars, Gaia 1 has experienced some level of s -process activity, as is reflected in a $[\text{Ba}/\text{Eu}]$ ratio of ~ 0.3 in out stars (Fig. 8). This is consistent with the broad range of this $[s/r]$ process indicator seen in disk field stars and star clusters at similar metallicities. Not surprisingly, Gaia 1 also overlaps with the thick disk ratios in this parameter space, while thin disk and bulge stars, at higher metallicities, show progressively higher s -process contributions towards the solar value. Here we note the interesting exception of the metal-rich ($[\text{Fe}/\text{H}] = -0.50$ dex) bulge GC NGC 6440, which has recently been exposed as a pure r -process system at $[\text{Ba}/\text{Eu}] \sim 0.65$ (Muñoz et al. 2017) with heavy element production being dominated by explosive nucleosynthesis, e.g., in SNe

II. This finding added to the complexity of this Galactic component, leading Muñoz et al. (2017) to suggest that the chemical enrichment of bulge GCs was special and may have been different from the remainder of the Galactic population.

5. Kinematics and orbit – Gaia 1 in the era of Gaia

5.1. Radial velocities and dynamic mass

Radial velocities were measured from a cross correlation of the heliocentrically corrected spectra against a typical red giant star template, yielding a precision of typically 0.3 km s^{-1} . The accuracy of the zeropoints in our wavelength scale was ascertained by cross correlating the telluric A- and B-bands against synthetic atmospheric spectra tailored to the sky conditions at the point of our observations, using the TAPAS (Transmissions Atmosphériques Personnalisées Pour l’Astronomie) simulator (Bertaux et al. 2014).

As a result, we established the mean heliocentric radial velocity of Gaia 1 as $57.2 \pm 1.5 \text{ km s}^{-1}$ with a dispersion of $\sigma = 3.0 \pm 1.1 \text{ km s}^{-1}$. While the mean value is in excellent agreement with that found by both Simpson et al. (2017) and Mucciarelli et al. (2017), our dispersion is larger by $\sim 2 \text{ km s}^{-1}$. Here, it is worth mentioning that, as discussed further in Sect. 5.2, the proper motions of all our four stars clearly associate them as cluster members, so there is no indication of a field star inflating the dispersion in velocities. In fact, this higher velocity dispersion appears to be driven by the higher radial velocity of member star #3. We cannot exclude the possibility that this object is in a binary, but a better temporal coverage of observations would be needed to confirm this.

Koposov et al. (2017) estimated the system’s luminous mass (down to $G < 19$ mag) to be $2.2 \times 10^4 M_{\odot}$ from their radial number density profile, adopting their best-fit isochrone and a initial mass function from Chabrier (2003) and assuming that mass follows light. Using our kinematic data we can attempt an independent measure of the cluster’s dynamic mass. A tentative value can be gleaned from the formalism of Illingworth (1976) as $M_{\text{dyn}} \sim 167 \mu \sigma^2 r_c$, where r_c refers to the core-radius and μ is the dimensionless mass, scaling with the object’s concentration (King 1966). By assuming Gaia 1’s half-light radius of $9 \pm 0.6 \text{ pc}$ as an upper limit for r_c and its full extent from the profile of Koposov et al. (2017), this yields a consistent value of $M_{\text{dyn}} = (3^{+4}_{-2}) \times 10^4 M_{\odot}$. In turn, using the prescription of Spitzer (1987) in terms of the better-defined half-light radius, i.e., $M_{\text{dyn}} = 9.75 r_h \sigma^2 / G$, where G is the gravitational constant, yields a larger value of $(1.8 \pm 1.4) \times 10^5 M_{\odot}$. While still broadly consistent with the luminous mass within the uncertainties, this value would rather imply the presence of a dark matter component in Gaia 1, more in line with its being a dwarf galaxy than a “simple” star cluster (Mateo et al. 1993; Walker et al. 2007; Gilmore et al. 2007). Alternatively, Gaia 1 could have been a formerly more massive system that had lost a great deal of its initial mass. This would render the occurrence of a spread in Fe and/or multiple populations in this object a viable possibility (Carretta et al. 2009a; Koch et al. 2012; Kirby et al. 2013). However, this interpretation hinges on the measured, large velocity dispersion: adopting a lower value of $(0.94 \pm 0.15) \text{ km s}^{-1}$ (Simpson et al. 2017) renders the mass lower by a factor of ten, at $(1.8 \pm 0.6) \times 10^4 M_{\odot}$. Given the low number of targets involved, we will not place further weight on these mass arguments.

Overall, within the error our finding is compatible with the low dispersions found in other GCs of comparable mass. Here, we note that the works of Pryor & Meylan (1993) and Harris

(1996, 2010 edition) only list one object, Pal 13, that is fainter than Gaia 1 with a measured velocity dispersion (Côté et al. 2002; Blecha et al. 2004). Similarly, OCs exhibit low intrinsic dispersions (Friel 2013) below 10 km s^{-1} , with a tendency of increasing values for older systems (Hayes & Friel 2014).

5.2. Proper motions and orbit

As in our previous work on largely uncharted star clusters (Koch et al. 2017), we computed the orbits of our four target stars using proper motions from the UCAC5 catalog (Zacharias et al. 2017). Using the *Gaia*-TGAS stars in the 8 to 11 magnitude range a reference star catalog, the UCAC5 catalog released new proper motions for the high quality, ground-based US Naval Observatory CCD Astrograph Catalog (UCAC) all-sky observations on the *Gaia* coordinate system. This allows the UCAC5 proper motions to be similar in performance to the *Gaia*-TGAS ones, but for a much larger sample of stars – over 107 million stars have proper motion measurements with typical accuracies of 1 to 2 mas yr^{-1} . The UCAC5 proper motions are, in general, improved compared those presented in TGAS. Fig. 9 shows the UCAC5 proper motions for all UCAC5 sources centred on Gaia 1, within a $7.5'$ arcmin radius. The stars presented here, as well as those observed by Simpson et al. (2017) and Mucciarelli et al. (2017), are also shown. It is clear that the proper motion estimated by Simpson et al. (2017) – by combining the *Gaia* and 2MASS positional information – is offset from the mean UCAC5 proper motions of the cluster stars. All of our stars have proper motions consistent with cluster membership, as do the Mucciarelli et al. (2017) stars, albeit their star #3 which they discarded due to damped absorption lines and a marginally different radial velocity.

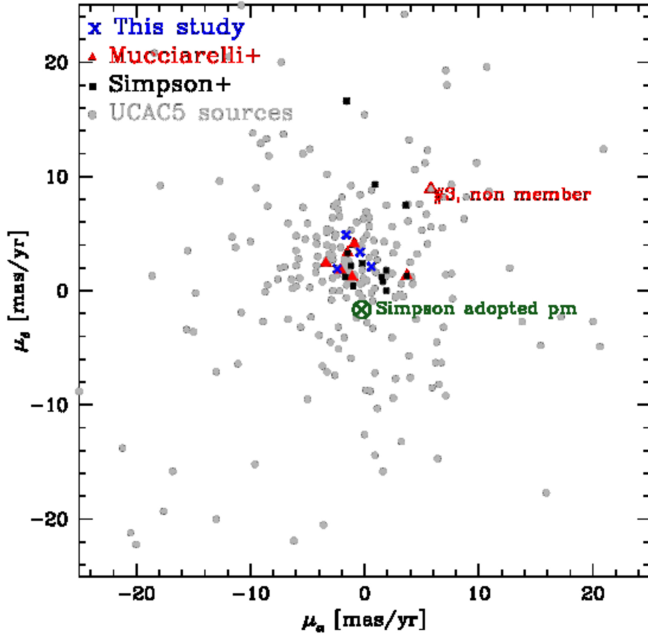


Fig. 9. Proper motions of stars within $7.5'$ of Gaia 1. Spectroscopic targets from Simpson et al. (2017), Mucciarelli et al. (2017), and our work are highlighted.

Owing to our spectroscopically derived gravities, we derived distances to our stars, further adopting isochrones that reflect our measured metallicities. The resulting heliocentric distance

of $4.1 \pm 1.1 \text{ kpc}$ is broadly consistent with the value found by Koposov et al. (2017) of 4.6 kpc from sparse photometry. The derived orbits below depend only mildly on the distance adopted and the errors in orbital parameters are chiefly driven by proper motion errors. Our star #4 has the largest formal proper motion uncertainty of 1.9 mas yr^{-1} , whereas the others have proper motion uncertainties between 1.2 and 1.4 mas yr^{-1} .

Using the *galpy* Python package⁵ and the recommended *MWPotential2014* potential with the default parameters (Bovy 2015), we integrated the orbit backwards in time for 10 Gyr. The resulting orbit projections are shown in Fig. 9. As expected for open clusters, the stars show quasi-periodic crown orbits.

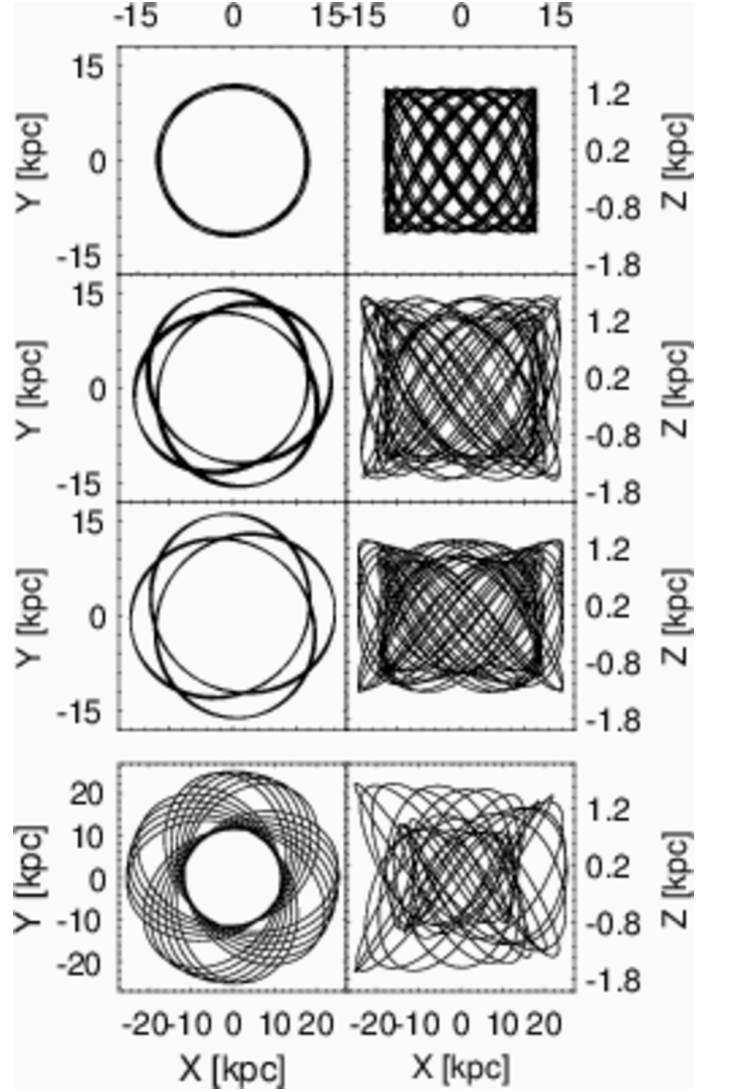


Fig. 10. Orbit projection of stars #1–4 (top to bottom).

The mean eccentricity of our stars is 0.14, which is an ellipticity value that coincides with the peak of thick-disk eccentricity distribution from $\sim 30\,000$ thick disk stars presented in Dierickx et al. (2010). It is, however, also consistent with a thin disk eccentricity, as the range between 0.1 to 0.3 is the eccentricity regime in which the thin and thick-disk stars overlap (Lee et al. 2011; Boechse et al. 2013). Our eccentricity gives Gaia 1 a considerably rounder orbit than that derived by Simpson et al.

⁵ <http://github.com/jobovy/galpy>; version 1.2

(2017). The eccentricity is largely insensitive to the actual distance within a 0.5 kpc range, so the factor of two difference between the eccentricity found here and that presented in Simpson et al. (2017) is almost entirely due to the different proper motions used (see also Figure 9).

Importantly, because our orbital ellipticity is half the size of the ellipticity calculated by Simpson et al. (2017), the radial quantity η (see also Vande Putte et al. 2010) invoked by Simpson et al. (2017) to argue for an extra-galactic origin of this cluster, is also half the size as that found by these authors. We find $\eta = 0.24$, which is well inline with a typical open cluster, especially considering its metallicity, as more metal-poor open clusters tend to have larger η values. Moreover, the maximum height above the Galactic plane, Z_{\max} resulting from our integration reaches ~ 1.0 kpc for the four stars, which is in line with the scale height of the thick disk, but in contrast to the larger value of 1.7 kpc found by those authors. Unfortunately the Z_{\max} depends more strongly on the adopted distance as compared to eccentricity, so this parameter is more uncertain. Still, taken together with the above discussion, we do not find strong evidence that Gaia 1 has a particularly anomalous orbit.

Fig. 11 shows a Toomre diagram of Galactic stars (left panel) that have been kinematically tagged as thin disk, thick disk, or halo stars by Reddy et al. (2003, 2006) and Bensby et al. (2014). Similarly, the right panel includes kinematic measurements of Galactic OCs (Vande Putte et al. 2010) that were divided into the Galactic components following the prescription of Bensby et al. (2014). While also the OC connection with a thick disk seems feasible, Vande Putte et al. (2010) assigned properties to their kinematic cluster sample based on orbital eccentricity and maximum height above the plane, which are likely correlated with age and metallicity of the systems. As such, Gaia 1 would qualify as a system that either was accreted into the disk from an extragalactic source, or it resulted from a merger of proto-cluster material with high-latitude gas clouds. This has already been suggested by (Simpson et al. 2017), although an extragalactic origin has been excluded by the chemical abundance study of Mucciarelli et al. (2017). However, as our present work opened up the possibility of an abundance spread in this system, such an origin cannot fully be discarded anymore. Given that only $\sim 5\%$ of open clusters are associated with the thick disk (Holmberg et al. 2007; Wu et al. 2009), the statistical samples to understand these systems are just not as large. Our chemo-dynamical tagging of Gaia 1 was finally able to ascertain its present association with the thick disk, whereas its exact formation and origin remains ambiguous.

6. Conclusions

Chemical tagging of stellar populations has proven indispensable when the underlying details of the cluster in question are sparse. Even the addition of a handful of spectroscopic measurements of candidate member stars can often establish a unique association of an object with either of the Galactic components. This was recently exemplified by the low-mass GC ESO452-Sc11 (Bica et al. 1999), which Koch et al. (2017) chemically tied to the Galactic bulge.

Likewise, settling an accurate abundance scale for stellar systems is imperative for deriving their ages. In this context, views about the nature of the target of the present work, Gaia 1, are ambivalent. This is also in part because the distance to the cluster is poorly constrained – for example, the main sequence turn-off, which has considerable power to discriminate between isochrones, has not clearly been imaged yet. The discovery of

Gaia 1 implied an intermediate isochrone-age and metallicity of 6.3 Gyr and -0.7 dex (Koposov et al. 2017). In contrast, first spectroscopic analyses (Simpson et al. 2017; Mucciarelli et al. 2017) led to an age of 3 Gyr based on CaT and EW measurements plus spectral synthesis at similar resolution to ours, albeit with smaller wavelength coverage. The resulting $[\text{Fe}/\text{H}]$ was higher by more than half a dex than our values from a high-resolution abundance analysis, which returned metallicities in line with the preliminary colour-magnitude diagram fitting.

Our abundance analysis revealed α -abundances that are consistent with the thick disk, consolidated by the neutron-capture elements and finally bolstered by the stars' kinematics. Despite the presence of mild light element variations in Na, Mg, and Al no obvious (anti-)correlations are seen between those elements as would be expected in Galactic GCs. Since its stellar mass of a few ten thousand M_{\odot} places Gaia 1 at the boundary between very low-mass GCs and very luminous OCs, our analysis rather comforts the latter view, as already suggested by the CMD study of Koposov et al. (2017). Thus, our chemo-dynamical tagging of Gaia 1 enabled us to clearly ascertain its present association with the thick disk and rather being a massive OC than a low-mass GC. However, the hint of a metallicity spread between different studies in the literature may point towards a more complex origin that could involve a once more massive progenitor. Thus the question as to its exact formation and origin remains unclear and needs to await more data such as the precise and accurate parallaxes that *Gaia* can offer.

Acknowledgements. We are grateful to the referee, Piercarlo Bonifacio, for a very helpful and thorough report that helped to better understand the discrepancies with the literature. This work was supported in parts by Sonderforschungsbereich SFB 881 "The Milky Way System" (subproject A8) of the German Research Foundation (DFG). This work has made use of data from the European Space Agency (ESA) mission *Gaia* (<https://www.cosmos.esa.int/gaia>), processed by the *Gaia* Data Processing and Analysis Consortium (DPAC, <https://www.cosmos.esa.int/web/gaia/dpac/consortium>). Funding for the DPAC has been provided by national institutions, in particular the institutions participating in the *Gaia* Multilateral Agreement.

References

- Alonso, A., Arribas, S., & Martínez-Roger, C. 1999, *A&AS*, 140, 261
- Asplund, M., Grevesse, N., Sauval, A. J., & Scott, P. 2009, *ARA&A*, 47, 481
- Battistini, C. & Bensby, T. 2016, *A&A*, 586, A49
- Bensby, T., Feltzing, S., & Oey, M. S. 2014, *A&A*, 562, A71
- Bensby, T., Yee, J. C., Feltzing, S., et al. 2013, *A&A*, 549, A147
- Bergemann, M. & Cescutti, G. 2010, *A&A*, 522, A9
- Bergemann, M., Pickering, J. C., & Gehren, T. 2010, *MNRAS*, 401, 1334
- Bertaux, J. L., Lallement, R., Ferron, S., Boonne, C., & Bodichon, R. 2014, *A&A*, 564, A46
- Bica, E., Ortolani, S., & Barbuy, B. 1999, *A&AS*, 136, 363
- Blecha, A., Meylan, G., North, P., & Royer, F. 2004, *A&A*, 419, 533
- Boeche, C., Chiappini, C., Minchev, I., et al. 2013, *A&A*, 553, A19
- Bovy, J. 2015, *ApJS*, 216, 29
- Bragaglia, A., Gratton, R. G., Carretta, E., et al. 2012, *A&A*, 548, A122
- Busso, M., Gallino, R., & Wasserburg, G. J. 1999, *ARA&A*, 37, 239
- Carretta, E., Bragaglia, A., Gratton, R., D'Orazi, V., & Lucatello, S. 2009a, *A&A*, 508, 695
- Carretta, E., Bragaglia, A., Gratton, R., & Lucatello, S. 2009b, *A&A*, 505, 139
- Carretta, E., Bragaglia, A., Gratton, R. G., et al. 2010, *A&A*, 516, A55
- Castelli, F. & Kurucz, R. L. 2004, *ArXiv Astrophysics e-prints*
- Chabrier, G. 2003, *PASP*, 115, 763
- Chambers, K. C., Magnier, E. A., Metcalfe, N., et al. 2016, *ArXiv e-prints*
- Chen, L., Hou, J. L., & Wang, J. J. 2003, *AJ*, 125, 1397
- Côté, P., Djorgovski, S. G., Meylan, G., Castro, S., & McCarthy, J. K. 2002, *ApJ*, 574, 783
- Cunha, K., Frinchaboy, P. M., Souto, D., et al. 2016, *Astronomische Nachrichten*, 337, 922
- Cutri, R. M., Skrutskie, M. F., van Dyk, S., et al. 2003, *2MASS All Sky Catalog of point sources*.

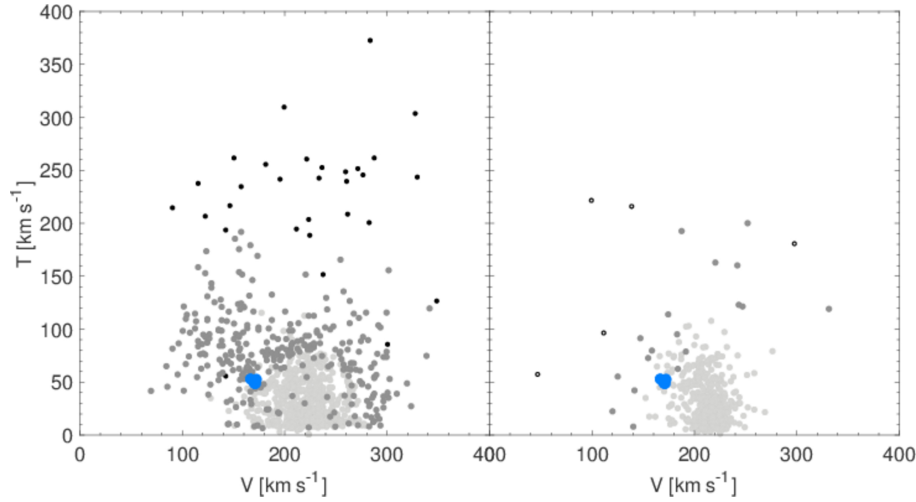


Fig. 11. Left panel: Toomre diagram of the kinematically separated literature samples and the Gaia 1 stars. As in the previous figures, light gray points are thin disk stars, dark gray ones are for the thick disk, and black symbols denote stars on halo-like orbits. The right panel uses OCs from the compilation of Vande Putte et al. (2010) as a comparison sample, colour-coded following the decomposition procedure of Bensby et al. (2014).

- Dierickx, M., Klement, R., Rix, H.-W., & Liu, C. 2010, *ApJ*, 725, L186
 Dotter, A., Chaboyer, B., Jevremović, D., et al. 2008, *ApJS*, 178, 89
 Feltzing, S. & Chiba, M. 2013, *New A Rev.*, 57, 80
 Freiburghaus, C., Rosswog, S., & Thielemann, F.-K. 1999, *ApJ*, 525, L121
 Friel, E. D. 2013, *Open Clusters and Their Role in the Galaxy*, ed. T. D. Oswalt & G. Gilmore, 347
 Geisler, D., Wallerstein, G., Smith, V. V., & Casetti-Dinescu, D. I. 2007, *PASP*, 119, 939
 Gilmore, G., Wilkinson, M. I., Wyse, R. F. G., et al. 2007, *ApJ*, 663, 948
 Gonzalez, O. A., Rejkuba, M., Zoccali, M., et al. 2011, *A&A*, 530, A54
 Hanke, M., Koch, A., Hansen, C. J., & McWilliam, A. 2017, *A&A*, 599, A97
 Hansen, C. J., Montes, F., & Arcones, A. 2014, *ApJ*, 797, 123
 Harris, W. E. 1996, *AJ*, 112, 1487
 Hayes, C. R. & Friel, E. D. 2014, *AJ*, 147, 69
 Holmberg, J., Nordström, B., & Andersen, J. 2007, *A&A*, 475, 519
 Illingworth, G. 1976, *ApJ*, 204, 73
 Janes, K. A. 1979, *ApJS*, 39, 135
 Johnson, C. I. & Pilachowski, C. A. 2010, *ApJ*, 722, 1373
 Johnson, C. I., Rich, R. M., Kobayashi, C., & Fulbright, J. P. 2012, *ApJ*, 749, 175
 Johnson, C. I., Rich, R. M., Kobayashi, C., Kunder, A., & Koch, A. 2014, *AJ*, 148, 67
 Karakas, A. I. & Lattanzio, J. C. 2014, *PASA*, 31, e030
 Kelson, D. D. 1998, PhD thesis, Univ. California at Santa Cruz, (1998)
 Kelson, D. D. 2003, *PASP*, 115, 688
 Kelson, D. D., Illingworth, G. D., van Dokkum, P. G., & Franx, M. 2000, *ApJ*, 531, 159
 King, I. R. 1966, *AJ*, 71, 64
 Kirby, E. N., Cohen, J. G., Guhathakurta, P., et al. 2013, *ApJ*, 779, 102
 Koch, A. & Edvardsson, B. 2002, *A&A*, 381, 500
 Koch, A., Hansen, C. J., & Kunder, A. 2017, *A&A*, 604, A41
 Koch, A., Lépine, S., & Çalişkan, Ş. 2012, in *European Physical Journal Web of Conferences*, Vol. 19, European Physical Journal Web of Conferences, 03002
 Koch, A. & McWilliam, A. 2008, *AJ*, 135, 1551
 Koch, A. & McWilliam, A. 2014, *A&A*, 565, A23
 Koch, A., McWilliam, A., Preston, G. W., & Thompson, I. B. 2016, *A&A*, 587, A124
 Koposov, S. E., Belokurov, V., & Torrealba, G. 2017, *MNRAS*, 470, 2702
 Lee, J.-W., Kang, Y.-W., Lee, J., & Lee, Y.-W. 2009, *Nature*, 462, 480
 Lee, Y. S., Beers, T. C., An, D., et al. 2011, *ApJ*, 738, 187
 Lind, K., Asplund, M., Barklem, P. S., & Belyaev, A. K. 2011, *A&A*, 528, A103
 Lind, K., Primas, F., Charbonnel, C., Grundahl, F., & Asplund, M. 2009, *A&A*, 503, 545
 Magain, P. 1984, *A&A*, 134, 189
 Magrini, L., Sestito, P., Randich, S., & Galli, D. 2009, *A&A*, 494, 95
 Marino, A. F., Milone, A. P., Karakas, A. I., et al. 2015, *MNRAS*, 450, 815
 Masseron, T., Plez, B., Van Eck, S., et al. 2014, *A&A*, 571, A47
 Mateo, M., Olszewski, E. W., Pryor, C., Welch, D. L., & Fischer, P. 1993, *AJ*, 105, 510
 Mauro, F., Moni Bidin, C., Cohen, R., et al. 2012, *ApJ*, 761, L29
 McWilliam, A. 2016, *PASA*, 33, e040
 Muñoz, C., Villanova, S., Geisler, D., et al. 2017, *A&A*, 605, A12
 Mucciarelli, A., Monaco, L., Bonifacio, P., & Saviane, I. 2017, *A&A*, 603, L7
 Navarro, J. F., Abadi, M. G., Venn, K. A., Freeman, K. C., & Anguiano, B. 2011, *MNRAS*, 412, 1203
 Ness, M., Freeman, K., Athanassoula, E., et al. 2013, *MNRAS*, 430, 836
 Nissen, P. E., Chen, Y. Q., Carigi, L., Schuster, W. J., & Zhao, G. 2014, *A&A*, 568, A25
 Nissen, P. E., Chen, Y. Q., Schuster, W. J., & Zhao, G. 2000, *A&A*, 353, 722
 Nissen, P. E. & Schuster, W. J. 2010, *A&A*, 511, L10
 Origlia, L., Massari, D., Rich, R. M., et al. 2013, *ApJ*, 779, L5
 Pancino, E., Carrera, R., Rossetti, E., & Gallart, C. 2010, *A&A*, 511, A56
 Pancino, E., Romano, D., Tang, B., et al. 2017, *A&A*, 601, A112
 Pehlivan Rhodin, A., Hartman, H., Nilsson, H., & Jönsson, P. 2017, *A&A*, 598, A102
 Placco, V. M., Frebel, A., Beers, T. C., & Stancliffe, R. J. 2014, *ApJ*, 797, 21
 Prusti, T., de Bruijne, J. H. J., Brown, A. G. A., et al. 2016, *A&A*, 595, A1
 Pryor, C. & Meylan, G. 1993, in *Astronomical Society of the Pacific Conference Series*, Vol. 50, Structure and Dynamics of Globular Clusters, ed. S. G. Djorgovski & G. Meylan, 357
 Recio-Blanco, A., de Laverny, P., Kordopatis, G., et al. 2014, *A&A*, 567, A5
 Reddy, A. B. S., Lambert, D. L., & Giridhar, S. 2016, *MNRAS*, 463, 4366
 Reddy, B. E., Lambert, D. L., & Allende Prieto, C. 2006, *MNRAS*, 367, 1329
 Reddy, B. E., Tomkin, J., Lambert, D. L., & Allende Prieto, C. 2003, *MNRAS*, 340, 304
 Rojas-Arriagada, A., Recio-Blanco, A., de Laverny, P., et al. 2017, *A&A*, 601, A140
 Ruchti, G. R., Feltzing, S., Lind, K., et al. 2016, *MNRAS*, 461, 2174
 Schlafly, E. F. & Finkbeiner, D. P. 2011, *ApJ*, 737, 103
 Simmerer, J., Sneden, C., Cowan, J. J., et al. 2004, *ApJ*, 617, 1091
 Simpson, J. D., De Silva, G. M., Martell, S. L., et al. 2017, *MNRAS*, 471, 4087
 Sneden, C., Cowan, J. J., & Gallino, R. 2008, *ARA&A*, 46, 241
 Sneden, C. A. 1973, PhD thesis, The University of Texas at Austin.
 Spite, F. & Spite, M. 1982, *A&A*, 115, 357
 Spitzer, L. 1987, *Dynamical evolution of globular clusters*
 Van der Swaelmen, M., Barbay, B., Hill, V., et al. 2016, *A&A*, 586, A1
 Vande Putte, D., Garnier, T. P., Ferreras, I., Mignani, R. P., & Cropper, M. 2010, *MNRAS*, 407, 2109
 Walker, M. G., Mateo, M., Olszewski, E. W., et al. 2007, *ApJ*, 667, L53
 Woosley, S. E. & Weaver, T. A. 1995, *ApJS*, 101, 181
 Wright, E. L., Eisenhardt, P. R. M., Mainzer, A. K., et al. 2010, *AJ*, 140, 1868
 Wu, Z.-Y., Zhou, X., Ma, J., & Du, C.-H. 2009, *MNRAS*, 399, 2146
 Zacharias, N., Finch, C., & Frouard, J. 2017, *AJ*, 153, 166